SCIENTIFIC REPORTS

OPEN

SUBJECT AREAS:
BATTERIES
ENERGY
SOLID-STATE CHEMISTRY
SUSTAINABILITY

Received
19 March 2013

Accepted
20 May 2013

Published
5 June 2013

Correspondence and requests for materials should be addressed to X.F.Z. (zhouxf@nimte.ac.cn) or Z.P.L. (liuzp@nimte.ac.cn)

New-concept Batteries Based on Aqueous Li^+/Na^+ Mixed-ion Electrolytes

Liang Chen, Qingwen Gu, Xufeng Zhou, Saixi Lee, Yonggao Xia & Zhaoping Liu

Ningbo Institute of Materials Technology and Engineering, Chinese Academy of Sciences, Ningbo 315201, P. R. China.

Rechargeable batteries made from low-cost and abundant materials operating in safe aqueous electrolytes are attractive for large-scale energy storage. Sodium-ion battery is considered as a potential alternative of current lithium-ion battery. As sodium-intercalation compounds suitable for aqueous batteries are limited, we adopt a novel concept of Li^+/Na^+ mixed-ion electrolytes to create two batteries ($LiMn_2O_4/Na_{0.22}MnO_2$ and $Na_{0.44}MnO_2/TiP_2O_7$), which relies on two electrochemical processes. One involves Li^+ insertion/extraction reaction, and the other mainly relates to Na^+ extraction/insertion reaction. Two batteries exhibit specific energy of 17 Wh kg^{-1} and 25 Wh kg^{-1} based on the total weight of active electrode materials, respectively. As well, aqueous $LiMn_2O_4/Na_{0.22}MnO_2$ battery is capable of separating Li^+ and Na^+ due to its specific mechanism unlike the traditional "rocking-chair" lithium-ion batteries. Hence, the Li^+/Na^+ mixed-ion batteries offer promising applications in energy storage and Li^+/Na^+ separation.

The increasing deployment of renewable energy sources such as solar and wind power requires a commensurate increase in energy storage capacity to integrate them into the grid. Batteries are good means of storing the electricity in the form of chemical energy. Owning to good safety, high ionic conductivity and low cost, aqueous rechargeable batteries are potentially advantageous over their organic counterparts for large-scale energy storage[1].

Various aqueous batteries such as alkaline Zn-MnO_2, lead-acid, nickel-metal hydride (Ni-MH), and nickel-metal (e.g., cadmium, iron, zinc and cobalt) are commercially available or under extensive research[1–6]. Alkaline Zn/MnO_2 is a primary battery; lead-acid and Ni-Cd batteries suffer from serious environmental problems because of the highly poisoning metals of lead and cadmium; Ni-MH is expensive due to the utilization of rare earth elements; Ni-Co, Ni-Fe and Ni-Zn batteries have poor cycling stability. These drawbacks in above systems hinder their utilization for large-scale energy storage. Recently, a variety of aqueous metal-ion batteries (e.g., Li^+, Na^+, K^+ and Zn^{2+} etc.) on a basis of metal-ion intercalation chemistry have garnered great interests[7–18]. Aqueous "rocking-chair" lithium-ion batteries using the cathode materials adopted from organic electrolyte cells (e.g., $LiMn_2O_4/VO_2$, $LiMn_2O_4/LiV_3O_8$, $LiMn_2O_4/TiP_2O_7$, $LiMn_2O_4/LiTi_2(PO_4)_3$, and $LiFePO_4/LiTi_2(PO_4)_3$ etc.) have been developed, but in general they exhibited limited cycle life[7–10]. A study by Xia's group showed that the cycling stability could be raised to a commercially level by eliminating O_2, controlling the pH of electrolytes, and cabon-coating the electrode materials[10]. Cui et al. reported a novel potassium-ion battery using carbon/polypyrrole hybrid (AC-PPy) anode and copper hexacyanoferrate (CuHCF) cathode, which offered long cycle life and good rate capability[12]. A unique zinc-ion battery based on Zn anode, α-MnO_2 cathode and mild electrolytes was explored by Kang et al. It exhibited high capacity and fast charge/discharge capability[13].

In contrast to lithium, potassium and zinc, sodium is most abundant and economical. Therefore, sodium-based energy storage system is considered as a promising technology for large-scale energy storage. However, only a couple of materials have been reported for the deintercalation/intercalation of sodium ion in aqueous media[14–20]. The reason is that several side reactions are involved in aqueous media, such as electrode materials reacting with water or O_2, proton co-intercalation into the electrode materials parallel to the intercalation of sodium ion, H_2/O_2 evolution reactions, and the dissolution of electrode materials in water. Whitacre et al. found that sodium ion could be reversibly inserted into $Na_{0.44}MnO_2$, owning to its unique tunnel structure[14]. But it only delivered a specific capacity of 45 mAh g^{-1} at 0.125 C rate. Yamaki et al. investigated the electrochemical behavior of $NaTi_2(PO_4)_3$ in aqueous sodium electrolytes[15]. Its redox potential is -0.6 V vs. standard hydrogen electrode, indicating that $NaTi_2(PO_4)_3$ can be utilized as an anode for aqueous sodium battery. The aqueous "rocking-chair" sodium-ion battery consisted of $NaTi_2(PO_4)_3$ and $Na_{0.44}MnO_2$ was reported by both Whitacre's and Chiang's groups[16,17]. Cui et al. found that materials with the Prussian Blue crystal structure (copper and nickel hexacyanoferrate) contained large interstitial sites, which allowed for the insertion and extraction of Na^+ and/or K^+

(ref. 18,19). Their capacities were in the range of 50–60 mAh g^{-1}. In a word, much more work on the exploration of new sodium-intercalated materials is needed to make aqueous sodium batteries viable in the field of large-scale energy storage.

Since sodium-intercalated materials suitable for aqueous media are limited, an innovative concept of Li^+/Na^+ mixed-ion electrolytes is employed to construct rechargeable batteries, as shown in Fig. 1. In such batteries, one side involves the immigration of Li^+ between electrolytes and electrode, and the other one refers to the exchange of Na^+ between electrode and electrolytes. During charging and discharging, the total concentration of Li^+ and Na^+ is fixed to ensure the charge neutrality of the electrolytes, but the Li^+/Na^+ ratio is changed. They are unlike traditional "rocking-chair" lithium-ion battery on a basis of the immigration of Li^+ between cathode and anode. Herein, two systems based on Li_2SO_4/Na_2SO_4 mixed electrolytes ($LiMn_2O_4/Na_{0.22}MnO_2$ and $Na_{0.44}MnO_2/TiP_2O_7$), which to our best knowledge have never been reported before, are demonstrated. The capacity, operating voltage, and stability of such batteries are dependent on the electrolytes. A $LiMn_2O_4/Na_{0.22}MnO_2$ system to separate Li^+ and Na^+ based on the unique mechanism of mixed-ion battery is also validated.

Results

Characterizations of $Na_{0.44}MnO_2$, $LiMn_2O_4$ and TiP_2O_7. The detailed synthetic procedures of above three materials are described in Methods. Manganese oxides form a rich structural family enlisting materials with either 1D-, 2D-, 3D-type tunnel structure. Among them, $Na_{0.44}MnO_2$ belongs to the space group *Pbam* with orthorhombic structure (see Supplementary Fig. S1). The manganese ions are located in two different environments: all Mn^{4+} ions and half of the Mn^{3+} ions are in octahedral sites, while the other Mn^{3+} gathered in a square-pyramidal environment. The latter forms edge-linked chains linked to two double and one triple octahedral chain by the vertices, leading to the formation of two types of tunnels (S-shaped tunnel and pentagon tunnel). The sites in S-shaped tunnel are approximately half-filled, and the sites in pentagon tunnel are almost fully occupied. Ab initio studies shows that half of sodium ions can be reversibly inserted into $Na_{0.44}MnO_2$ in the range of −0.10–0.85 V vs. saturated calomel electrode (SCE), resulting in a theoretical capacity of 60 mAh g^{-1} (ref. 19). X-ray diffraction (XRD) pattern of the $Na_{0.44}MnO_2$ powders in Supplementary Fig. S1 shows five strong peaks at 14.2°, 16.8°, 19.7°, 34.2° and 37.6°, responding to the reflections of (130), (140), (150), (280) and (151) plane of orthorhombic structure, respectively[21,22]. In addition, no peaks related to Mn_2O_3 impurity are detectable[14,22]. The particles are also well crystallized and have grown anisotropically, leading to nanorod shape. The nanorods show an excellent atomic ordering, and always exhibit (110) crystal plane with interplanar distance of 0.87 nm (Supplementary Fig. S1).

Spinel $LiMn_2O_4$ has 3D tunnel structure with space group *Fd3m*. The Mn ions have an octahedral coordination to the oxygen atoms, and the MnO_6 octahedra share edges in a 3D host for the Li guest ions (Supplementary Fig. S2). Proton can also diffuse into the tunnel due to its small ion radius. XRD pattern of synthesized $LiMn_2O_4$ powders confirms a pure spinel phase. Scanning electron microscopy (SEM) analysis shows that the powders are composed of microspheres (Supplementary Fig. S2).

Pyrophosphate TiP_2O_7 has a cubic $3 \times 3 \times 3$ superstructure with space group *Pa3*. It consists of TiO_6 octahedral and PO_4 tetrahedral sharing corners in a 3D network (Supplementary Fig. S3). Such framework can accommodate Li^+ insertion and extraction, leading to a theoretical capacity of 121 mAh g^{-1}. Carbon-coated TiP_2O_7 with a pure cubic phase is synthesized through solid state reaction method (see method and Supplementary Fig. S3). It exhibits a highly dispersed particulate morphology. High resolution TEM image of TiP_2O_7 particle displays that amorphous carbon with average thickness of 7 nm is uniformly coated on the surface of the particle (Supplementary Fig. S3). The amount of carbon in the materials is about 16%, which is estimated by thermogravimetric analysis.

Selectivity of $Na_{0.44}MnO_2$ for Na^+ against Li^+. The electrochemical properties of prepared $Na_{0.44}MnO_2$ in different electrolytes are investigated by cyclic voltammetry (CV) and galvanostatic techniques. Fig. 2a displays three reversible redox couples at ca. 0.05, 0.28 and 0.46 V vs. SCE in aqueous Na_2SO_4 electrolytes, corresponding to the insertion and extraction of Na^+ (ref. 13 and 20). In Li_2SO_4/Na_2SO_4 mixed electrolytes, these redox couples still exist, but their potentials are different from the ones in Na_2SO_4 electrolytes. In Li_2SO_4 electrolytes, three irreversible oxidation peaks at 0.08 V, 0.31 V, and 0.49 V, attributed to the removal of Na^+ from $Na_{0.44}MnO_2$, are observed in the first cycle. Very weak peaks related to Li^+ insertion and extraction are seen in the subsequent cycles. It concludes that only a very small amount of Li^+ can be reversibly inserted/de-inserted into/from $Na_{0.44}MnO_2$, regardless of its smaller ionic radius (76 pm) compared to Na^+ (102 pm). Moreover, Na^+ can be selectively extracted and inserted

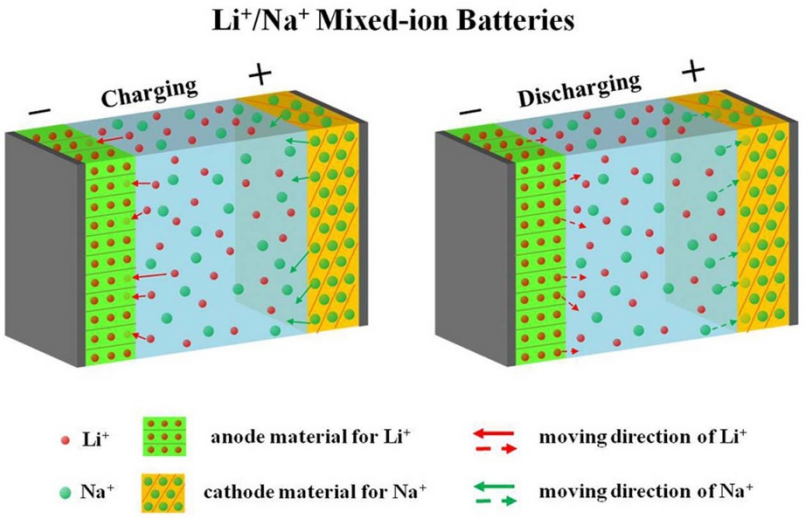

Figure 1 | Schematics of Li^+/Na^+ mixed-ion battery. Lithium-intercalation compounds and sodium-intercalation compounds are used for anode and cathode, respectively. During charging (or discharging), the storage (or release) of Li^+ takes place at anode, and the release (or storage) of Na^+ occurs at cathode.

from/into $Na_{0.44}MnO_2$ in the presence of Li^+ and $Na_{0.44}MnO_2$ exhibits high selectivity of Na^+ towards Li^+. Between −0.1 and 0.65 V vs. SCE, the discharge capacities of $Na_{0.44}MnO_2$ in 1 M Na_2SO_4, 1 M Na_2SO_4 + 0.125 M Li_2SO_4, 1 M Na_2SO_4 + 0.25 M Li_2SO_4 and 1 M Na_2SO_4 + 0.5 M Li_2SO_4 electrolytes are 62.1, 60.7, 60.2 and 57.9 mAh g^{-1} at 0.25 C rate (1 C = 60 mAh g^{-1}), respectively (Supplementary Fig. S4). These values are much larger than 45 mAh g^{-1} obtained by Whitacre's group, and agree well with the theoretical capacity of 60 mAh g^{-1}, which indicate that about half of sodium ions in $Na_{0.44}MnO_2$ can be reversibly intercalated into tunnels of $Na_{0.44}MnO_2$ in mixed electrolytes. The unique nanorod shape and good crystallinity of $Na_{0.44}MnO_2$ may account for its high capacity and good reversibility. It is also found that the capacity slightly decreases with an increase of the Li^+/Na^+ ratio.

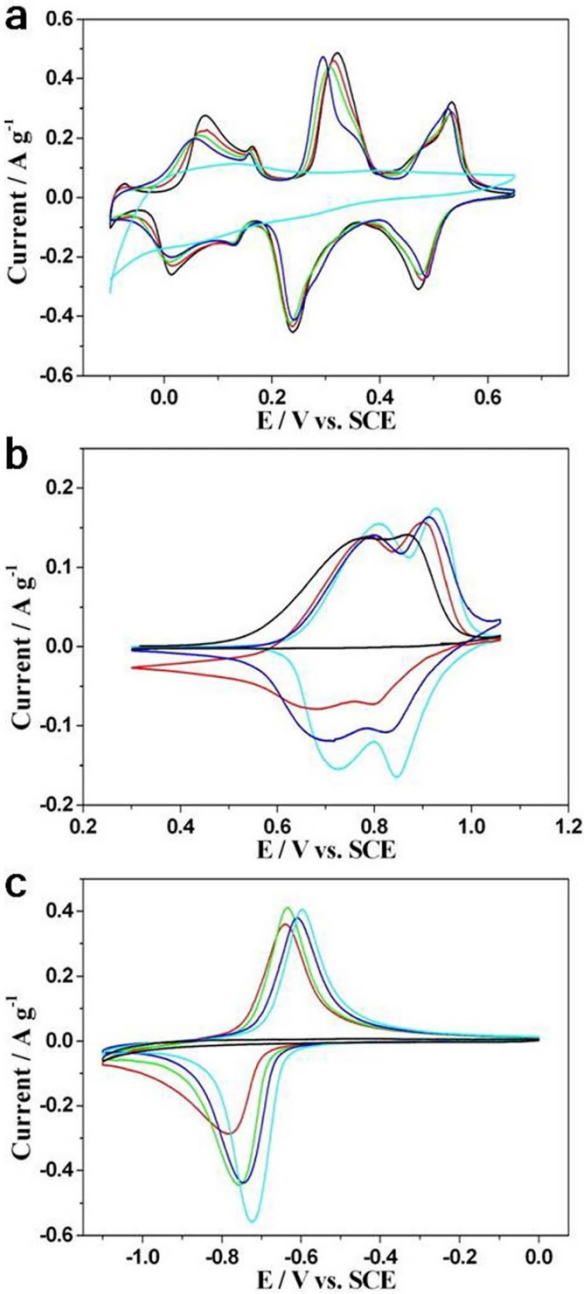

Figure 2 | Cyclic voltammograms in different electrolytes. (a), for $Na_{0.44}MnO_2$ electrode at a scan rate of 0.5 mVs^{-1}. (b), for $LiMn_2O_4$ electrode at a scan rate of 0.1 mVs^{-1}. (c), for carbon-coated TiP_2O_7 electrode at a scan rate of 0.3 mVs^{-1}. Black line: in 1 M Na_2SO_4; red line: in 1 M Na_2SO_4 + 0.125 M Li_2SO_4; green line: in 1 M Na_2SO_4 + 0.25 M Li_2SO_4; blue line: in 1 M Na_2SO_4 + 0.5 M Li_2SO_4; cyan line: in 1 M Li_2SO_4.

Selectivity of $LiMn_2O_4$ and TiP_2O_7 for Li^+ against Na^+. Fig. 2b describes the CV curves of $LiMn_2O_4$ in different electrolytes. In Li_2SO_4 electrolytes, two pairs of redox peaks locate at 0.81 V and 0.93 V (oxidation potential vs. SCE), indicating two-phase lithium extraction/insertion behavior inherent to spinel $LiMn_2O_4$. In mixed electrolytes, the redox peaks still exist, but their potentials and currents are relatively lower than the ones in Li_2SO_4 electrolytes. However, only two irreversible oxidation peaks are seen in Na_2SO_4 electrolytes, indicating that Na^+ can hardly diffuse into bulk $LiMn_2O_4$. Meanwhile, the peak potential decreases by decreasing the Li^+/Na^+ ratio, as expected from kinetics consideration. The kinetics of the insertion and extraction are strongly influenced by lithium concentration. During Li^+ insertion reaction, a decrease in lithium concentration results in a decrease of the limiting diffusion current and therefore an increase of the concentration overvoltage, which results in a negative shift of the peak potential. In terms of Li^+ extraction reaction, a decrease in lithium concentration leads to an easier removal of Li^+ from bulk $LiMn_2O_4$, which also shifts the peak potential towards smaller value. It is also observed that both the potential of charge/discharge plateau and the capacity decrease with decreasing the Li^+/Na^+ ratio (see Supplementary Fig. S4).

Similar lithium ion sieve property is observed for TiP_2O_7. Fig. 2c shows the CV curves of TiP_2O_7 in different electrolytes. In Li_2SO_4 electrolytes, a pair of Li^+ intercalation and extraction peaks appear at −0.72V and −0.60 V vs. SCE[23]. In mixed electrolytes, the peak potential decreases with a decrease of the Li^+/Na^+ ratio. Similar trend is seen for the $LiMn_2O_4$ material. No redox peaks are observed in Na_2SO_4 electrolytes, implying that TiP_2O_7 can only store and release Li^+. The charging/discharging capacities between 0 V and −0.9 V vs. SCE in mixed electrolytes are close to the one in Li_2SO_4 electrolytes, indicating that Na^+ has no obvious effect on the capacity of TiP_2O_7 (Supplementary Fig. S4). The coulombic efficiency in 1 M Li_2SO_4, 1 M Na_2SO_4 + 0.5 M Li_2SO_4, 1 M Na_2SO_4 + 0.25 M Li_2SO_4 and 1 M Na_2SO_4 + 0.125 M Li_2SO_4 electrolytes are 86.7%, 81.3%, 91.3% and 82.5%, respectively. All of them are much lower than the theoretical one of 100%. It may be mainly caused by the decomposition of water and trace of oxygen in the electrolytes. According to Nernst equation, the theoretical H_2 evolution potential at pH = 7 locates at −0.66 V vs. SCE, the same as the redox potential of Ti^{3+}/Ti^{4+} in TiP_2O_7 (−0.66 V vs. SCE). It means that the evolution of H_2 may be parallel to the insertion of Li^+ into TiP_2O_7 during discharging. Negative electrode candidates for aqueous lithium-ion battery are found to be sensitive to oxygen and water on the discharged-state[10]. The potential of charge/discharge plateau decreases with decreasing the Li^+/Na^+ ratio, which is consistent with the phenomena observed from CV experiments.

$LiMn_2O_4/Na_{0.22}MnO_2$ and $Na_{0.44}MnO_2/TiP_2O_7$ batteries. Based on the above mixed-ion chemistry of $Na_{0.44}MnO_2$, $LiMn_2O_4$ and TiP_2O_7, we assembled two practical prototypes of mixed-ion batteries ($LiMn_2O_4/Na_{0.22}MnO_2$ and $Na_{0.44}MnO_2/TiP_2O_7$). Fig. 3a illustrates the principle of $LiMn_2O_4/Na_{0.22}MnO_2$ system ($Na_{0.22}MnO_2$ is obtained through electrochemical oxidation of $Na_{0.44}MnO_2$). One side mainly involves the immigration of Na^+ between electrolytes and $Na_{0.22}MnO_2$, and the other side is related to the insertion/extraction of Li^+ into/from $LiMn_2O_4$. Typical charge-discharge curves of $LiMn_2O_4/Na_{0.22}MnO_2$ battery in two different electrolytes are displayed in Fig. 3b and 3c. Such a battery can deliver a capacity of 29 mAh g^{-1} (0.25 C rate) based on the total mass of active materials between 0.2 V and 1.05 V. The coulombic efficiency of the battery after the first cycle is above 90%, indicating its good reversibility. Fig. 3d shows the plot of discharging capacity retention percentage vs. the cycle number. In both electrolytes, the fading rate of the

capacity in the initial 10 cycles is much higher than the one after 10 cycles. After 45 cycles, 83% of the original capacity is remained in 1 M Na_2SO_4 + 0.125 M Li_2SO_4. But in 1 M Na_2SO_4 + 0.5 M Li_2SO_4, the capacity remains only 61% of the original one. Therefore, its cycling stability can be enhanced by decreasing the Li^+/Na^+ ratio. The rate performance of $LiMn_2O_4/Na_{0.22}MnO_2$ battery in 1 M Na_2SO_4 + 0.125 M Li_2SO_4 is also tested. The discharge capacities of 27.9, 25.5, 19.2, 11.7 and 7.7 mAh g^{-1} are obtained at 0.5, 1, 2, 4 and 8 C rate, respectively (see Supplementary Fig. S5).

The principle of the mixed-ion battery comprised by a TiP_2O_7 anode and a $Na_{0.44}MnO_2$ cathode is described in Fig. 4a. As shown, the Li^+ insertion and removal take place at anode, and the release and storage of Na^+ occur at cathode. Fig. 4b and 4c depict charge-discharge profiles of $Na_{0.44}MnO_2/TiP_2O_7$ battery in two different electrolytes. The operating voltage of the battery ranges from 0.65 V to 1.3 V. And the voltage of charging/discharging plateau in 1 M Na_2SO_4 + 0.125 M Li_2SO_4 is 30 mV–40 mV higher than the one in 1 M Na_2SO_4 + 0.25 M Li_2SO_4. Between 0.65 V and 1.3 V, the battery can give reversible capacities of 23.5 mAh g^{-1} in 1 M Na_2SO_4 + 0.25 M Li_2SO_4 and 25.0 mAh g^{-1} in 1 M Na_2SO_4 + 0.125 M Li_2SO_4 at 0.4 C rate. Meanwhile, it exhibits good coulombic efficiency after the first cycle (> 96%) in both electrolytes, which is indicative of good reversibility of the battery. Its cycling stability is studied as well. The fading rate of discharging capacity is much higher in the first 10 cycles than the one after 10 cycles (see Fig. 4d). Similar phenomena are also observed for $LiMn_2O_4/Na_{0.22}MnO_2$ system. In 1 M Na_2SO_4 + 0.125 M Li_2SO_4 electrolytes, 83% and 62% of the original discharging capacity are retained after 10 and 50 cycles, respectively. In the case of 1 M Na_2SO_4 + 0.25 M Li_2SO_4 electrolytes, only 76% and 58% of the original discharging capacity are remained. As a result, raising the Na^+/Li^+ ratio can improve the cycling stability of $Na_{0.44}MnO_2/TiP_2O_7$ battery. A discharge rate capability study of $Na_{0.44}MnO_2/TiP_2O_7$ battery in 1 M Na_2SO_4 + 0.125 M Li_2SO_4 is shown in Supplementary Fig. S5. The discharge capacities of 23.3, 20.6, 17.7, 14.5 and 11.1 mAh g^{-1} are found at 0.5, 1, 2, 4 and 8 C rate, respectively.

Elucidation on the mechanism of Li^+/Na^+ mixed-ion batteries. The feature of mixed-ion battery is the changes of Li^+/Na^+ ratio during charging and discharging. To experimentally demonstrate such changes, a micro electrochemical cell consisted of a $Na_{0.22}MnO_2$ anode and a $LiMn_2O_4$ cathode is made. We choose several electrolytes to study (see Table 1). Firstly, Na_2SO_4 and Li_2SO_4 solution are selected. Before charging, pristine Na_2SO_4 solution with the Li^+/Na^+ ratio of 1/83 is injected into the cell. After charging, the Li^+/Na^+ ratio goes up to 1/10. This is due to the release of Li^+ from a $LiMn_2O_4$ cathode, and selective capture of Na^+ from electrolytes by a $Na_{0.22}MnO_2$ anode. In contrast, Li_2SO_4 solution replaces Na_2SO_4 solution for the discharging process. The Li^+/Na^+ ratio in electrolytes drops from 144/1 to 13/1 after discharging. The reason is that Li^+ in electrolytes is intercalated into cathode, and Na^+ is diffused from anode to electrolytes during discharging. Similar changes are also observed for mixed-ion solutions. The Li^+/Na^+ ratio increases after charging, and decreases after discharging. Therefore, $LiMn_2O_4/Na_{0.22}MnO_2$ system can enrich Li^+ in electrolytes by charging, and enrich Na^+ by discharging.

Discussion

Li^+/Na^+ mixed-ion batteries are based on the ion-selectivity of electrode materials. As demonstrated by the electrochemical data,

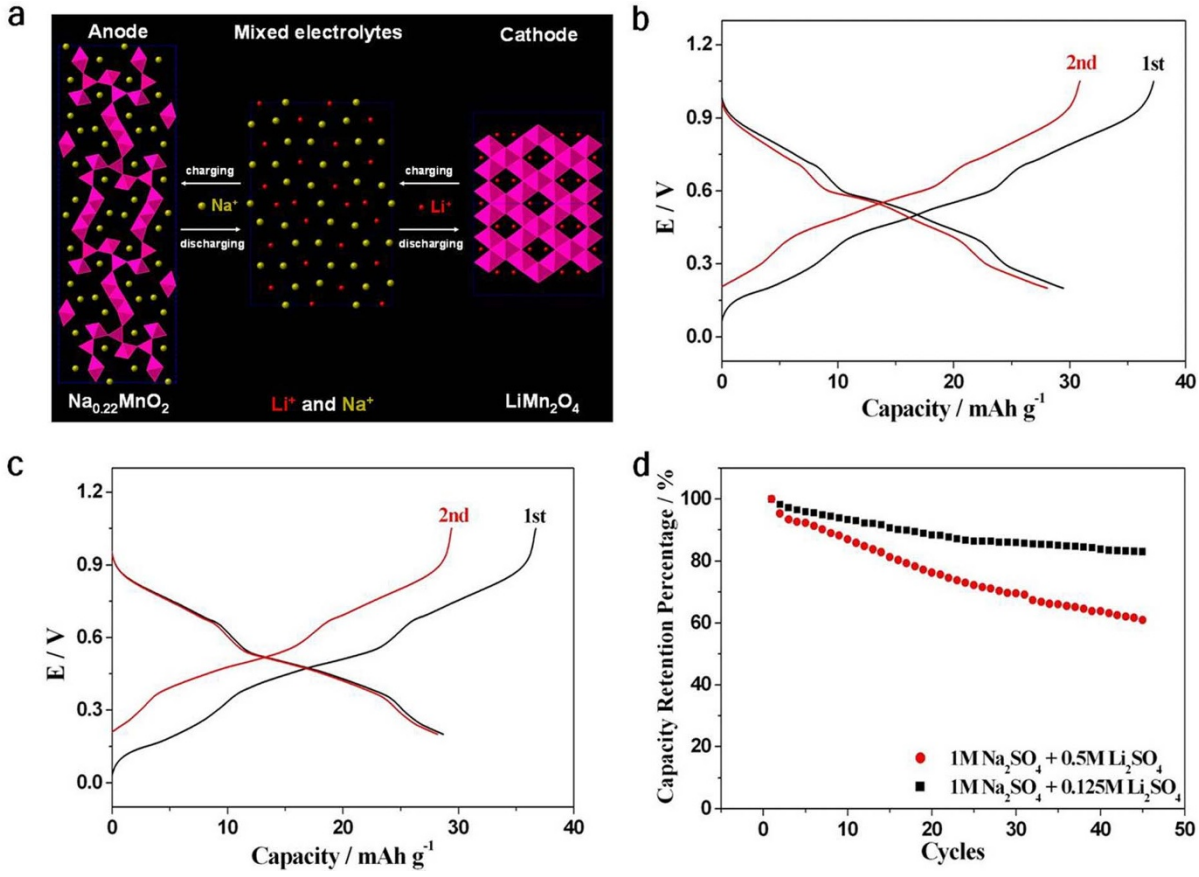

Figure 3 | The $LiMn_2O_4/Na_{0.22}MnO_2$ mixed-ion battery. (a), A schematic of the battery. (b), Charging-discharging curves at a rate of 0.25 C in 1 M Na_2SO_4 + 0.5 M Li_2SO_4. (c), Charging-discharging curves at a rate of 0.25 C in 1 M Na_2SO_4 + 0. 125 M Li_2SO_4. (d), Cycle life tests of the battery at a rate of 0.25 C in mixed electrolytes. (1 C = 60 mAh g^{-1}).

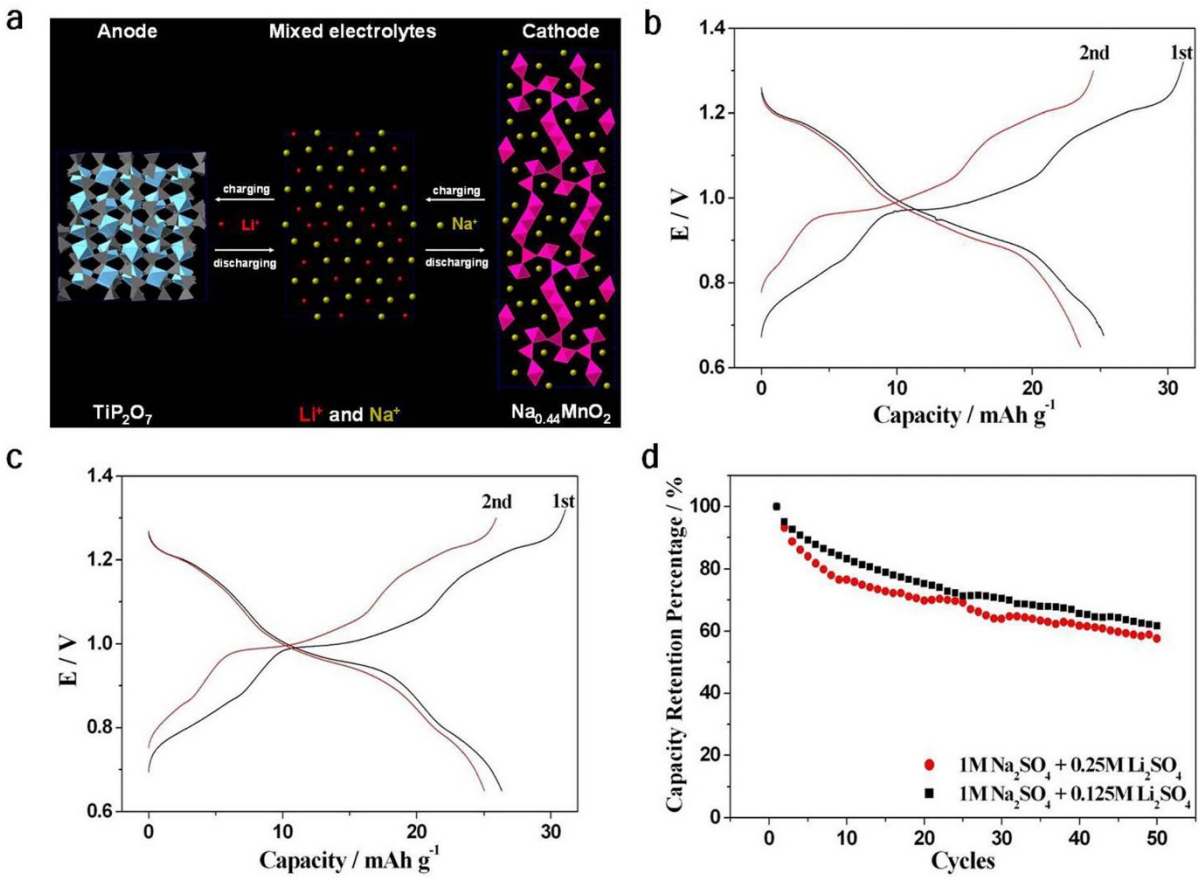

Figure 4 | The $Na_{0.44}MnO_2/TiP_2O_7$ mixed-ion battery. (a), A schematic of the battery. (b), Charging-discharging curves at a rate of 0.4 C in 1 M Na_2SO_4 + 0.25 M Li_2SO_4. (c), Charging-discharging curves at a rate of 0.4 C in 1 M Na_2SO_4 + 0. 125 M Li_2SO_4. (d), Cycle life tests of the battery at a rate of 0.4 C in mixed electrolytes. (1 C = 60 mAh g^{-1}).

$Na_{0.44}MnO_2$, $LiMn_2O_4$ and TiP_2O_7 exhibit specific ion-selectivity. Their ion-selectivity has also been confirmed by the X-ray photoelectron spectroscopy experiments (see Supplementary Table S1). In Li^+/Na^+ mixed-ion solutions, $Na_{0.44}MnO_2$ exhibits specific ion-selectivity towards Na^+. The reason may be the dimensions of two tunnels in $Na_{0.44}MnO_2$ (S-shaped tunnel and pentagon tunnel) are too large for Li^+ to be anchored. The mismatch leads to the free movement of Li^+ in the tunnels. Both $LiMn_2O_4$ and TiP_2O_7 behave as ion sieves which exhibit very high ion-selectivity towards Li^+. Their specific selectivity can be easily explained by the steric effect: the tunnels are too small for metal ions with ionic radii larger than Li^+ to enter.

The theoretical capacities of $Na_{0.44}MnO_2$, $LiMn_2O_4$ and TiP_2O_7 are 60 mAh g^{-1}, 148 mAh g^{-1} and 121 mAh g^{-1}, respectively. The average working voltages of $LiMn_2O_4/Na_{0.22}MnO_2$ and $Na_{0.44}MnO_2/TiP_2O_7$ batteries are 0.6 V and 1.0 V. If the theoretical capacities of $Na_{0.44}MnO_2$, $LiMn_2O_4$ and TiP_2O_7 are fully used, batteries with specific energy of ca. 21 Wh kg^{-1} or 40 Wh kg^{-1} based on the total weight of active electrode materials could be desired. Thus the $Na_{0.44}MnO_2/TiP_2O_7$ system can be superior to CuHCF/AC-PPy and $Na_{0.44}MnO_2$/active-carbon systems for large-scale energy storage[12,14]. Actually, two batteries with specific energy of 17 Wh kg^{-1} and 25 Wh kg^{-1} are obtained in our work. How to achieve the theoretical capacities of these compounds and long cycle life of the systems still remains a challenge.

More and more lithium is needed to meet for the evermore demanding market of electric cars. As of 2012, most of the lithium

Table 1 | Atomic ratio of Li^+/Na^+ in the electrolytes during charging and discharging

	$[Li^+]/[Na^+]$			
Electrolytes	before charging	after charging	before discharging	after discharging
Na_2SO_4[a]	1 : 83	1 : 10	N.A.	N.A.
Li_2SO_4[b]	N.A.	N.A.	144 : 1	13 : 1
Li_2SO_4+Na_2SO_4[a]	100 : 42[c]	100 : 35	N.A.	N.A.
	100 : 35[d]	100 : 29	N.A.	N.A.
Li_2SO_4 + Na_2SO_4[b]	N.A.	N.A.	47 : 100[c]	41 : 100
	N.A.	N.A.	41 : 100[d]	36 : 100

Charging/discharging current density: 1 $mAcm^{-2}$. Voltage cutoff: 0.1 V and 1.05 V.
[a]Electrolytes for charging step.
[b]Electrolytes for discharging step.
[c]Electrolytes used for cycle 1.
[d]Electrolytes (obtained after cycle 1) used for cycle 2.
N.A.: not available.

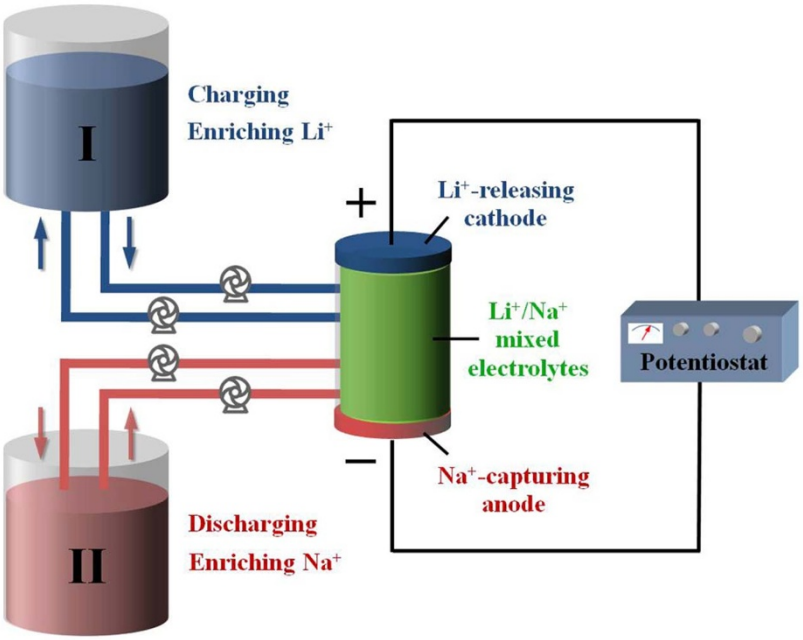

Figure 5 | Schematic representation of the working principle on the separation of Li^+ and Na^+ by the mixed-ion battery.

(roughly 83%) is obtained from brine lakes and salt pans. Existing methods for purification of lithium ("line soda evaporation process", amorphous Al_2O_3 process, and ion exchange technique) are wet chemistry techniques[24,25]. As such methods require a large quantity of chemicals (e.g., Na_2CO_3, $AlCl_3$, manganese oxides and HCl etc), they are expensive, slow and inefficient. Therefore, to explore new efficient methods for the recovery of lithium from brine is necessary. Based on the demonstrated mechanism of Li^+/Na^+ mixed-ion batteries, a new electrochemical method is proposed. Fig. 5 schematically shows the working principle of mixed-ion battery system for Li^+/Na^+ separation. The battery is based on the Li^+-releasing cathode and Na^+-capturing anode. During the first step (charging), the battery releases Li^+ and captures Na^+ to enrich Li^+ in mixed-ion solution I. After charging, the solution I is replaced by another mixed-ion solution II. Then the battery is discharged to enrich Na^+, as Li^+ are captured by cathode and Na^+ are released from anode. In the last step, mixed-ion solution II is exchanged with mixed-ion solution I for the next cycle. Throughout repetitive cycles, Li^+-enriched and Na^+-enriched solutions are finally obtained respectively. Compared with other purification methods as stated above, this method presents the following two evident advantages. Firstly, it is dual-functional. Li^+/Na^+ mixed-ion battery can be used for both purification of lithium and energy storage. Secondly, this electrochemical method is green and energy efficient. Unlike wet chemical methods, it does not require any chemicals and generates zero waste for disposal. To verify the feasibility of the method, the $LiMn_2O_4/Na_{0.22}MnO_2$ system is selected. Two mixed electrolytes are used as shown in Table 1. Firstly, $Li_2SO_4+Na_2SO_4$ solution with the Li^+/Na^+ ratio of 100/42 (solution I) is added into the cell. After charging, the Li^+/Na^+ ratio goes up to 100/35. Then solution I is removed and substituted by another solution (solution II) for the next step. After discharging, the Li^+/Na^+ ratio in solution II decreases from 47/100 to 41/100. Subsequently, the $LiMn_2O_4/Na_{0.22}MnO_2$ battery is subjected to the second cycle. After two cycles, the Li^+/Na^+ ratio in solution I increases to 100/29, and the Li^+/Na^+ ratio in solution II drops to 36/100. These results demonstrates that Li^+/Na^+ mixed-ion battery can be applied for separating Li^+ and Na^+.

In summary, a unique "mixed-ion electrolytes" strategy is successfully used to establish Li^+/Na^+ mixed-ion batteries with the cathode/anode systems such as $LiMn_2O_4/Na_{0.22}MnO_2$ and $Na_{0.44}MnO_2/TiP_2O_7$. The resultant batteries are built on the ion-selective properties of $Na_{0.44}MnO_2$, $LiMn_2O_4$ and TiP_2O_7. The capacities, operating voltage and stability of both batteries are dependent on the Na^+/Li^+ ratio. Raising the Na^+/Li^+ ratio is beneficial to their stabilities. As well, $LiMn_2O_4/Na_{0.22}MnO_2$ system can be used to separate Li^+ and Na^+. In a word, Li^+/Na^+ mixed-ion batteries not only pave a new route to the energy storage system, but also give a prospective technique for Li^+/Na^+ separation.

Methods

Material syntheses. All chemicals were obtained from Sinopharm Chemical Reagent Co., Ltd (Shanghai, China). $Na_{0.44}MnO_2$ and $LiMn_2O_4$ were prepared by solid-state reaction method. To make $Na_{0.44}MnO_2$ nanorods, Na_2CO_3 was ball milled with $MnCO_3$ in a 0.25 : 1 ratio at 350 rpm for 8 h. The precursor mix was successively heated for 3 h at 300°C and for 9 h at 800°C. For spherical $LiMn_2O_4$, starting materials $MnCO_3$ and Li_2CO_3 were thoroughly mixed in a molar ratio of 4 : 1. The mixture was hand-grounded, pelletized, and heated at 800°C in air for 12 h. The as-prepared TiP_2O_7 samples were also synthesized by solid-state reaction routine. The high purity TiO_2 powder (up to 99.9%) and $NH_4H_2PO_4$ were added into ethanol to form paste. This paste was ball-milled in a planetary ball mill at 400 rpm for 8 h. After ball milling, the mixture was dried at 80°C to evaporate ethanol. Then it was successively heated for 5 h at 300°C and for 12 h at 900°C under air with intermediate grindings. The obtained white TiP_2O_7 solids, referred as as-prepared TiP_2O_7, were homogenized in a mortar for further use. For carbon-coated TiP_2O_7, 2.5 g of as-prepared TiP_2O_7, 2 g of glucose and appropriate amount of ethanol were mixed and then ball-milled for 4 h. The solids were obtained by evaporating the ethanol at 80°C. After calcined at 700°C for 5 h in Ar, the solids became black, implying that TiP_2O_7 were coated by carbon.

Characterizations. Powder X-ray diffraction patterns were collected using an AXS D8 Advance diffractometer (Cu Kα radiation; receiving slit, 0.2 mm; scintillation counter, 40 mA; 40 kV) from Bruker Inc. The morphology and structure of samples were analyzed by a Hitachi S-4800 field emission scanning-electron microscope and an FEI Tecnai G2 F20 transmission electron microscope at an accelerating voltage of 200 kV. Thermal gravimetric analysis was performed on a Pyris Diamond thermogravimetric/differential thermal analyzer by Perkin-Elmer. Elemental analyses were carried out on inductively coupled plasma optical emission spectrometer (Perkin Elmer Optima 2100 DV).

Electrochemical measurements. Electrochemical measurements were carried on Solartron 1470E multi-channel potentiostats using either two-electrode or three-electrode cell. For three-electrode setup, saturated calomel electrode (SCE) and Pt gauze were employed as reference and counter electrodes, respectively. Both cathode and anode were prepared by casting slurries of active materials (75 wt%), Super P (15 wt%) and polyvinylidene fluoride (10 wt%) in n-methyl-2-pyrrolidinone on steel iron grid, and air drying at 80°C for 12 h. Disks of diameter (1.3 cm) were cut for electrochemical tests. Mass loadings for the electrodes were determined by comparing

the mass of the electrode with that of the original blank one. $Na_{0.22}MnO_2$ electrodes were fabricated through electrochemical oxidation of $Na_{0.44}MnO_2$ electrodes (constant current: 30 mAg^{-1}, cut-off voltage: 0.65 V vs. SCE). Deaerated solutions obtained through Ar gas bubbling for 60 min were used for TiP_2O_7 electrodes. The mass ratios of anode to cathode materials are designed as 1.80 for $LiMn_2O_4$/$Na_{0.22}MnO_2$ system and 0.85 for $Na_{0.44}MnO_2$/TiP_2O_7 system, according to the capacities of $Na_{0.44}MnO_2$, $LiMn_2O_4$, and carbon-coated TiP_2O_7. A micro electrochemical cell consisted of a $Na_{0.22}MnO_2$ anode and a $LiMn_2O_4$ cathode was fabricated to test the change of Li^+/Na^+ ratio during charging and discharging. The distance between two electrodes was fixed at 2.2 mm. The volume of electrolytes was 1.0 mL and the total concentration of Li^+ and Na^+ was about 0.35 M. Inductively coupled plasma optical emission spectroscopy (ICP-OES) was used to determine the ratio of Li^+/Na^+.

1. Soloveichik, G. L. Battery technologies for large-scale stationary energy storage. *Annu. Rev. Chem. Biomol. Eng.* **2**, 503–527 (2011).
2. Shen, Y. W. & Kordesch, K. The mechanism of capacity fade of rechargeable alkaline manganese dioxide zinc cells. *J. Power Sources* **87**, 162–166 (2000).
3. Shukla, A. K., Venugopalan, S. & Hariprakash, B. Nickel-based rechargeable batteries. *J. Power Sources* **100**, 125–148 (2001).
4. Köhler, U., Antonius, C. & Bäuerlein, P. Advances in alkaline batteries. *J. Power Sources* **127**, 45–52 (2004).
5. Wang, H. L. *et al.* An ultrafast nickel–iron battery from strongly coupled inorganic nanoparticle/nanocarbon hybrid materials. *Nat. Commun.* **3**, 917 (2012).
6. Gao, X. P., Yao, S. M., Yan, T. Y. & Zhou, Z. Alkaline rechargeable Ni/Co batteries: Cobalt hydroxides as negative electrode materials. *Energy Environ. Sci.* **2**, 502–505 (2009).
7. Li, W., Dahn, J. R. & Wainwright, D. S. Rechargeable lithium batteries with aqueous electrolytes. *Science* **264**, 1115–1118 (1994).
8. Wang, G. J. *et al.* An aqueous rechargeable lithium battery with good cycling performance. *Angew. Chem. Int. Ed.* **46**, 295–297 (2007).
9. Wang, H. B., Huang, K. L., Zeng, Y. Q., Yang, S. & Chen, L. Q. Electrochemical properties of TiP_2O_7 and $LiTi_2(PO_4)_3$ as anode material for lithium ion battery with aqueous solution electrolyte. *Electrochim. Acta.* **52**, 3280–3285 (2007).
10. Luo, J. Y., Cui, W. J., He, P. & Xia, Y. Y. Raising the cycling stability of aqueous lithium-ion batteries by eliminating oxygen in the electrolyte. *Nat. Chem.* **2**, 760–765 (2010).
11. Wang, X. J., Hou, Y. Y., Zhu, Y. S., Wu, Y. P. & Holze, R. An aqueous rechargeable lithium battery using coated Li metal as anode. *Sci. Rep.* **3**, 1401 (2013).
12. Pasta, M., Wessells, C. D., Huggins, R. A. & Cui, Y. A high-rate and long cycle life aqueous electrolyte battery for grid-scale energy storage. *Nat. Commun.* **3**, 1149 (2012).
13. Xu, C. J., Li, B. H., Du, H. D. & Kang, F. Y. Energetic zinc ion chemistry: The rechargeable zinc ion battery. *Angew. Chem. Int. Ed.* **51**, 933–935 (2012).
14. Whitacre, J. F., Tevar, A., & Sharma, S. $Na_4Mn_9O_{18}$ as a positive electrode material for an aqueous electrolyte sodium-ion energy storage device. *Electrochem. Commun.* **12**, 463–466 (2010).
15. Park, S. I., Gocheva, I., Okada, S. & Yamaki, J. I. Electrochemical properties of $NaTi_2(PO_4)_3$ anode for rechargeable aqueous sodium-ion batteries. *J. Electrochem. Soc.* **158**, A1067–A1070 (2011).
16. Wu, W., Mohamed, A. & Whitacre, J. F. Microwave synthesized $NaTi_2(PO_4)_3$ anode materials for rechargeable aqueous electrolyte sodium-ion battery. *Meet. Abstr.* 1859 (2012). (222nd ECS meeting, Honolulu, Hawaii).
17. Li, Z., Young, D., Xiang, K., Caeter, W. C. & Chiang, Y. M. Towards high power high energy aqueous sodium-ion batteries: The $NaTi_2(PO_4)_3$/$Na_{0.44}MnO_2$ system. *Adv. Energy Mater.* **3**, 290–294 (2013).
18. Wessells, C. D., Huggins, R. A. & Cui, Y. Copper hexacyanoferrate battery electrodes with long cycle life and high power. *Nat. Commun.* **2**, 550 (2011).
19. Wessells, C. D., Peddada, S. V., McDowell, M. T., Huggins, R. A. & Cui, Y. The effect of insertion species on nanostructured open framework hexacyanoferrate battery electrodes. *J. Electrochem. Soc.* **159**, A98–A103 (2012).
20. Wu, X. Y., Cao, Y. L., Ai, X. P., Qian, J. F. & Yang, H. X. A low-cost and environmentally benign aqueous rechargeable sodium-ion battery based on $NaTi_2(PO_4)_3$-$Na_2NiFe(CN)_6$ intercalation chemistry. *Electrochem. Commun.* **31**, 145–148 (2013).
21. Kim, H. *et al.* Ab initio study of the sodium intercalation and intermediate phases in $Na_{0.44}MnO_2$ for sodium-ion battery. *Chem. Mater.* **24**, 1205–1211 (2012).
22. Sauvage, F., Laffont, L., Tarascon, J. M. & Baudrin, E. Study of the insertion/deinsertion mechanism of sodium into $Na_{0.44}MnO_2$. *Inorg. Chem.* **46**, 3289–3294 (2007).
23. Patoux, S. & Masquelier, C. Lithium insertion into titanium phosphates, silicates, and sulfates. *Chem. Mater.* **14**, 5057–5068 (2002).
24. Garrett, D. E. *Handbook of Lithium and Natural Calcium Chlorides: Their Deposits, Processing, Uses and Properties.* Elsevier Academic Press, Amsterdam, Boston, 2004.
25. Ammundsen, B., Jones, D. J., Roziere, J. & Burns, G. R. Mechanism of proton insertion and characterization of the proton sites in lithium manganate spinels. *Chem. Mater.* **7**, 2151–2160 (1995).

Acknowledgements

We acknowledge the financial support from Key Research Program of Chinese Academy of Sciences (Grant No. KGZD-EW-202-4), Ningbo Science and Technology Innovation Team (Grant No. 2012B82001) and the 973 Program (Grant No. 2011CB935900).

Author contributions

L.C., Z.X. and Z.L. designed experiments. L.C., Q.G. (Joint graduate student from Department of Chemistry and Engineering, Huainan Normal University, P. R. China), and S.L. carried out experiments. L.C., X.Z., Z.L. and Y.X. contributed data analysis and co-wrote the paper. Z.L. and X.Z. proposed and supervised the project.

Additional information

Supplementary information accompanies this paper at http://www.nature.com/scientificreports

Competing financial interests: The authors declare no competing financial interests.

How to cite this article: Chen, L. *et al.* New-concept Batteries Based on Aqueous Li^+/Na^+ Mixed-ion Electrolytes. *Sci. Rep.* **3**, 1946; DOI:10.1038/srep01946 (2013).